

Further Developments in Rapidly Decelerating Turbulent Pipe Flow Modeling

S. Meniconi¹, H.F. Duan², M. ASCE, B. Brunone³, M. ASCE, M.S. Ghidaoui⁴, P.J. Lee⁵, M. ASCE, and M. Ferrante⁶

¹ Assistant Professor, Dipartimento di Ingegneria Civile e Ambientale, The University of Perugia, Via G. Duranti 93, 06125 Perugia, Italy. Email: silvia.meniconi@unipg.it.

² Assistant Professor, Department of Civil and Environmental Engineering, Hong Kong Polytechnic University, Hung Hom, Kowloon, Hong Kong.
Email: hf.duan@polyu.edu.hk. (*author for correspondence*)

³ Professor, Dipartimento di Ingegneria Civile e Ambientale, The University of Perugia, Via G. Duranti 93, 06125 Perugia, Italy. Email: bruno.brunone@unipg.it.

⁴ Chair Professor, Department of Civil and Environmental Engineering, The Hong Kong University of Science and Technology, Clear Water Bay, Kowloon, Hong Kong. Email: ghidaoui@ust.hk.

⁵ Senior Lecturer, Department of Civil and Natural Resources Engineering, The University of Canterbury, Private Bag 4800 Christchurch, New Zealand. Email: pedro.lee@canterbury.ac.nz.

⁶ Associate Professor, Dipartimento di Ingegneria Civile e Ambientale, The University of Perugia, Via G. Duranti 93, 06125 Perugia, Italy. Email: marco.ferrante@unipg.it.

Abstract: In the last two decades, energy dissipation in unsteady-state pressurized pipe flow has been examined by various authors, where the instantaneous wall shear stress is split into a quasi-steady and an unsteady shear stress component. The focus of most past studies is on formulating expressions for the unsteady wall shear stress, but there has been less work on the key parameters governing the dominance of unsteady friction in transient flows. This paper derives an expression for the head envelope damping for turbulent flows in smooth and rough pipes and provides new and carefully measured field data for the initial (i.e. pre-transient) Reynolds number, Re_0 , that ranges from 97000 to 380000. The analytical solution is derived on the basis of one-dimensional (1-D) waterhammer equations in which the unsteady component is represented by existing convolucional unsteady friction formulas for both smooth and rough turbulent sub-regimes. The analytical solution is used to formulate general, encompassing and theoretically-based dimensionless parameters to assess the importance of unsteady friction in comparison to the quasi-steady component. In addition, the analytical solution furnishes the similitude relations that allowed the damping behavior from existing laboratory tests, the field tests conducted as part of this research and the weighting function-based (WFB) models to be investigated and compared in a coherent manner in a single graph. The analysis confirms that the magnitude of Re_0 has a significant impact on the damping for transients generated by flow stoppage. In addition, the results show that convolucional unsteady friction model that uses the frozen eddy viscosity hypothesis and Re_0 has accuracy that decreases with time. An improvement for this shortcoming is proposed and

28 verified and involves the use of the instantaneous Reynolds number in lieu of the pre-
29 transient Reynolds number in the evaluation of the WFB models. The result is a modified
30 unsteady friction model that provides improved matches for both laboratory and field data
31 compared with the original model.

32 **Authors Keywords:** pressurized pipeline, turbulent flow, transients, unsteady friction, initial
33 conditions, smooth pipe, rough pipe

34

35 **Introduction**

36 Various authors in the past two decades have examined energy dissipation in unsteady-state
37 pressurized pipe (waterhammer) flows. The convention in the waterhammer literature is to
38 split the instantaneous wall shear stress, τ_w , into a sum of two components as follows,

$$39 \quad \tau_w = \tau_{ws} + \tau_{wu}, \quad (1)$$

40 where $\tau_{ws} = f \frac{\rho V |V|}{8}$ is the quasi-steady component with V , ρ and f being the
41 instantaneous mean flow velocity, fluid density and friction factor, respectively; and $\tau_{wu} =$
42 unsteady component. The formulation of τ_{wu} has been the topic of intense study and new
43 innovative approaches are continually being proposed in the literature (He and Jackson, 2000;
44 Axworthy *et al.* 2000, Zhao *et al.* 2007; He and Jackson, 2011; Storli and Nielsen, 2011a and
45 2011b, and Mitosek and Szymkiewicz, 2012). The proposed models can be broadly classified
46 into instantaneous acceleration-based (IAB) models (Brunone *et al.* 1991, 1995, 2004,
47 Bergant *et al.* 2001, Brunone and Golia 2008, and Pezzinga 2009) and weighting function-
48 based (WFB) models (Zielke 1968, Trikha 1975, Vardy and Brown 1995, 1996, 2003, 2004,
49 2010, Vitkovský *et al.* 2006, and Zarzycki, 2000). An indepth review of these models is
50 given in Ghidaoui *et al.* (2005).

51 A promising and popular type of physically-based unsteady friction model is based on
52 the WFB relations derived in Vardy and Brown (1995, 1996, 2003) for smooth-pipe flows
53 and in Vardy and Brown (2004) for rough pipe flows. These models involve the following
54 limiting assumptions: (i) the eddy viscosity is frozen to an idealized radial distribution whose
55 parameters are determined from the pre-transient flow conditions and (ii) the derivation of the
56 weighting function assumes that the fluid is incompressible. Therefore, it is important to
57 address the following questions: What is the range of validity of these models? How can they
58 be improved? When are these models required? Such questions have not received the
59 attention they deserve and only limited progress has been made towards answering them. For

60 example, Ghidaoui *et al.* (2002), and Duan *et al.* (2010, 2012) used a heuristic approach to
61 identify some key parameters that can determine the conditions under which unsteady
62 friction in transient flows is important. However, the approach used to arrive at the flow
63 parameters is heuristic and cannot distinguish between smooth and rough pipe turbulence.
64 The validity of WFB models is judged on the basis of comparison between measured and
65 computed head traces (e.g., Bergant *et al.* 2001, Ghidaoui and Mansour 2002, Stephens *et al.*
66 2005). However, the lack of theoretically derived similitude relations prevented (i) the
67 investigation of transient damping from different experiments and how this damping
68 compares with WFB in a general and consistent manner and (ii) the generation of knowledge
69 needed to propose improvement to existing WFB models.

70 This paper theoretically derives an expression for the head envelope damping for
71 turbulent flow in smooth and rough pipes and provides new and carefully measured field data.
72 The analytical solution provides general, encompassing and theoretically-based
73 dimensionless parameters, instead of the heuristically-based parameters in Ghidaoui *et al.*
74 (2002) and Duan *et al.* (2012), which can be used to assess the importance of unsteady
75 friction in comparison to the quasi-steady component. In addition, the analytical solution
76 furnishes the similitude relations that allow the damping behavior from existing laboratory
77 tests, the field tests conducted as part of this research and the WFB models to be investigated
78 and compared in a coherent manner in a single graph. As a result of this investigation, an
79 improvement to existing WFB models is proposed and tested.

80

81 **Further experiments on the role of Initial Reynolds Number**

82

83 ***Description of Laboratory and Field Experiments***

84 Experimental results were obtained from two separate sources to provide a rigorous test of
85 the unsteady friction damping across a wide range of Reynolds numbers. The laboratory
86 results are retrieved from Adamkowski and Lewandowski (2006) where the testing pipe
87 system is a single copper pipe with pipe length $L = 98.11$ m, $D = 16.0$ mm, and wall thickness
88 $e = 1.0$ mm. The Reynolds number of initial steady-state (Re_0 , with $Re = VD/\nu =$ Reynolds
89 number, $D =$ pipe diameter, $\nu =$ fluid kinematic viscosity, $L =$ pipe length, and the subscript 0
90 indicating the initial conditions) varies from 5.7×10^3 to 1.6×10^4 and the wavespeed, a , is
91 1298.4 m/s. Three tests from Adamkowski and Lewandowski (2006) are used for this study
92 and the parameters of these tests are shown in Table 1 as test cases no. 1 through 3, with the

93 measured pressure head, H , time-history – hereafter referred to as *pressure signal* – plotted
94 in Figs. 1 though 3, where t indicates time since valve closure. The initial steady-state
95 conditions of these three tests are smooth pipe flows.

96 Field tests were executed in the steel rising main connecting the Vallememoria well-
97 field and the SAB reservoir in Recanati, Italy, managed by ASTEA spa. The steel pipe has D
98 = 260 mm, $L = 4170$ m, and $a = 1210$ m/s and is supplied by three pumps installed in
99 parallel. The static head, H_s , is 260 m and a check valve is installed immediately downstream
100 of the pumping group. Note that all surge protection devices on the pipeline were deactivated.
101 The parameters of the field tests are shown in Table 1 as test cases no. 4 through 7. The tests
102 with the higher value of Re_0 were previously presented in Brunone *et al.* (2001, 2002).
103 Steady-state flow tests provided an estimate of the roughness height as $\varepsilon = 2.2$ mm. The
104 initial steady-state flow conditions of all the field tests in Table 1 are in the fully rough pipe
105 flow regime.

106 The pressure signal was measured immediately downstream of the check valve by a
107 strain gauge pressure transducer with a recording range up to 400 m, an accuracy of ± 2 m
108 and response time of 50 ms. The steady-state discharge was measured by a magnetic
109 flowmeter just upstream of the check valve. The transient signals from a pump trip and the
110 subsequent slamming of the check valve are shown in Figs. 4 through 7.

111

112 [add **Table 1** & **Figure 1** at this place]

113

114 *Analysis of the induced damping of pressure oscillations*

115 The crucial role of the Reynolds number for characterising uniform pipe flow emerged more
116 than a century ago between laminar and turbulent regimes. The laminar regime, which exists
117 for small values of Re , is analytically tractable and governed by the well-known Hagen-
118 Poiseuille relationship – in which the uniform wall shear stress, τ_w , is a function of V . On the
119 contrary, the turbulent regime is ungovernable by any analytical model and then friction is
120 evaluated by a myriad of empirical friction formulas where τ_w is a function of V^n , with
121 $1.75 \leq n \leq 2$ according to the turbulent subregime.

122 For the case of highly unsteady pipe flow, the first work that investigated the role of
123 Re_0 , is by Holmboe and Rouleau (1967). They considered the case of unsteady pipe flow
124 induced by a complete and fast closure of a valve placed at the downstream end of a single
125 pipe (i.e., constant diameter and supply head). They reported that when the initial flow was

126 unquestionably laminar, a noticeable distortion and damping of the pressure, H , occurred
 127 after the first half transient cycle. On the contrary, for larger values of Re_0 , the experimental
 128 pressure signals were quite similar to those given by the frictionless Allievi-Joukowsky
 129 theory. In Vardy and Brown (2003, 2004) the influence of Re_0 on the value of the unsteady
 130 friction coefficient has been pointed out for both smooth and rough pipe flow. Recently,
 131 Duan et al. (2012) has examined this problem more systematically by means of a simplified
 132 analytical model for smooth pipe, but their results have only been validated in a limited range
 133 of Re_0 by the experimental data from the literature.

134 In this section, numerical simulation is first applied to all the test cases to investigate
 135 the importance of unsteady friction as a function of Re_0 to further verify the results obtained
 136 in Duan et al. (2012) in a larger number of flow conditions. A 1-D method of characteristics
 137 model is used where only the effect of quasi-steady friction is considered (Ghidaoui et al.
 138 2005). The differences between the experiments and the model provide an indicative
 139 magnitude of the omitted unsteady friction effect in the experiments. The time traces between
 140 the numerical model and the experiments are compared in Figs. 1, 2, and 3 for the laboratory
 141 tests and in Figs. 4, 5, 6, and 7 for the field tests. In these figures the results from the
 142 numerical model is labeled as “ H_n ” and experimental data is labelled as “ H_e ”. It is also worth
 143 noting that the transient head for laboratory test cases no. 1 through 3 is defined by the
 144 difference between the total pressure head at the valve and the steady-state head at the
 145 upstream reservoir (constant head), so that after normalization the initially transient head
 146 response in Figs. 1 to 3 is smaller than 1. This definition of the transient head is consistent
 147 with the original publication by Adamkowski and Lewandowski (2006). The results show
 148 that the match between the model and the experiments improves with increasing Re_0 , which
 149 indicates that the importance of unsteady friction is decreasing with Reynolds number. This
 150 result is confirmed by the values of the determination coefficient, R^2 , which denotes the
 151 strength of the linear association between the experimental head response and the predicted
 152 head response from the quasi-steady 1-D model. The determination coefficient is defined as,

$$153 \quad R^2 = 1 - \frac{SS_{err}}{SS_{tot}} = 1 - \frac{\sum_i (y_i^e - y_i^n)^2}{\sum_i (y_i^e - \bar{y}_i^e)^2} \quad (2)$$

154 where SS_{err} = sum of squares of residuals, and SS_{tot} = total sum of squares (proportional to the
 155 sample variance), y_i^e = experimental value (with the overbar indicating the mean value), and
 156 y_i^n = numerical model value. A R^2 value closer to unity represents a more accurate model

157 prediction. The results of R^2 for all test cases in Table 1 are shown in Fig. 8. The trend of the
 158 determination coefficient in Fig. 8 is consistent with the results in Duan *et al.* (2012), which
 159 conclude that the importance of unsteady friction decreases with system scale and Re_0 .

160

161

[add **Figures 1 ~ 8** at this place]

162

163 Further insight into the behavior of the unsteady friction model can be found by
 164 deriving the envelope of the downstream pressure head and velocity oscillations for a single
 165 pipe where the downstream boundary valve is suddenly shut. The head and flow envelopes
 166 are given as follows (see derivation in Appendix I):

$$167 \quad H_{amp}(t) = \frac{aV_0}{g} e^{-K_{r0}\frac{t}{T_w}} = \frac{aV_0}{g} e^{-K_{rs0}\frac{t}{T_w}} e^{-K_{ru0}\frac{t}{T_w}} = \frac{aV_0}{g} e^{-K_{rs0}\left(1+\frac{K_{ru0}}{K_{rs0}}\right)\frac{t}{T_w}}, \quad (3)$$

168 and

$$169 \quad V_{amp}(t) = V_0 e^{-K_{r0}\frac{t}{T_w}} = V_0 e^{-K_{rs0}\frac{t}{T_w}} e^{-K_{ru0}\frac{t}{T_w}} = V_0 e^{-K_{rs0}\left(1+\frac{K_{ru0}}{K_{rs0}}\right)\frac{t}{T_w}}, \quad (4)$$

170 where subscript “amp” denotes amplitude, g = gravitational acceleration, K_{ru0} = damping rate
 171 due to unsteady friction, K_{rs0} = damping rate due to steady friction, $K_{r0} = K_{ru0} + K_{rs0}$ = total
 172 damping rate, and $T_w = L/a$ is wave timescale. The expressions of K_{r0} , K_{ru0} , and K_{rs0} for
 173 smooth pipe flow have been derived using the unsteady friction weighting functions of Vardy
 174 and Brown (1995, 1996, and 2003) in Duan *et al.* (2012). The parameters for fully rough pipe
 175 flow are derived using the unsteady friction model of Vardy and Brown (2004) in the present
 176 study (see Eqs. A22 and A23 in Appendix I).

177 According to Eqs. (3) and (4), the ratio K_{ru0}/K_{rs0} provides a measure for the relative
 178 importance of unsteady friction to steady friction. In particular, it is clear from the analytical
 179 solution that unsteady friction is not important when $K_{ru0}/K_{rs0} \ll 1$ and important otherwise.
 180 The expression for this ratio is given as below,

181 (i) for smooth pipe flow case:

$$182 \quad \frac{K_{ru0}}{K_{rs0}} = \begin{cases} \frac{2\sqrt{2}}{fRe_0} \sqrt{\frac{T_{dv}}{T_w}} & \text{if } Re_0 \frac{T_w}{T_{dv}} \ll 1 \\ \frac{0.066}{f(Re_0)^{1.94}} \left(\frac{T_{dv}}{T_w}\right)^2 & \text{otherwise} \end{cases} = \begin{cases} \frac{2\sqrt{2}}{f\sqrt{MRe_0}} \sqrt{\frac{D}{L}} & \text{if } M \frac{L}{D} \ll 1 \\ \frac{0.066}{f(Re_0)^{-0.06} M^2} \left(\frac{D}{L}\right)^2 & \text{otherwise} \end{cases}; \quad (5)$$

183 (ii) for rough pipe flow case:

184
$$\frac{K_{ru0}}{K_{rs0}} = 0.048 \left(\frac{\varepsilon}{D} \right)^{0.016} \left(\frac{T_{dv}}{T_w} \right)^{1.414} \frac{1}{fRe_0^{1.414}} = 0.048 \left(\frac{\varepsilon}{D} \right)^{0.016} \left(\frac{D}{L} \right)^{1.414} \frac{1}{fM^{1.414}}. \quad (6)$$

185 where $T_{dv} = D^2/\nu$ is viscous diffusion timescale.

186 It is clear from Eqs. (5) and (6) that the relative importance of the unsteady and quasi-
 187 steady components depends on (i) the pre-transient Reynolds number Re_0 , timescale ratio
 188 T_w/T_{dv} , Mach number M and L/D for smooth turbulent flows and (ii) Re_0 , T_w/T_{dv} , M , L/D and
 189 relative roughness ε/D for rough turbulent flows. Both Eqs. (5) and (6) support the finding of
 190 the last section in that $K_{ru0}/K_{rs0} \ll 1$ as Re_0 gets larger.

191 Table 1 provides the relevant parameters for the different test cases. The K_{ru0}/K_{rs0}
 192 column shows that the condition $K_{ru0}/K_{rs0} \ll 1$ is indeed valid for the test rigs for which the
 193 unsteady component is deemed irrelevant and K_{ru0}/K_{rs0} is of order 1 for the test rigs for which
 194 the unsteady component is deemed important. For example, $K_{ru0}/K_{rs0} = 1.19$ for case 1 which
 195 implies that the quasi-steady and unsteady component are of the similar importance and
 196 explains why the model which neglects the unsteady friction component provides poor
 197 agreement with the data as reported in Figure 1. In addition, both the analytical solution and
 198 Table 1 clearly show that the importance of unsteady friction diminishes with Re_0 . Moreover,
 199 the table also indicates the consistency between the values of the K_{ru0}/K_{rs0} column and the
 200 parameter I column, where $I = fRe_0 T_w/T_{dv} = fML/D$ as presented in Duan *et al.* (2012), where
 201 unsteady friction is deemed unimportant as I gets larger.

202

203 **Validity of Frozen Turbulence Hypothesis and Proposed Improvement to Existing WFB** 204 **Models**

205 The fact that the analytical solution of the pressure head damping presented in the previous
 206 section is only a function of Re_0 and not a time-dependent Reynolds number is largely an
 207 artifact of the frozen turbulence hypothesis used in the derivation of the friction model in
 208 Vardy and Brown (1995, 1996, 2003 and 2004). The ramifications of the frozen turbulence
 209 hypothesis are investigated below.

210 The damping from unsteady friction can be more elegantly represented by rewriting
 211 the pressure head envelope (H_{amp}) equation in Eq. (3) as follows:

212
$$\frac{1}{-K_{r0}} \ln \frac{gH_{amp}(t)}{aV_0} = \frac{t}{T_w}, \quad (7)$$

213 which shows that the pressure head envelope of all transient events, provided that the WFB
 214 unsteady friction model is valid, should collapse onto one single line. To test the validity of

215 equation and by implication the validity of the frozen turbulence hypothesis, the variations of
216 rescaled pressure envelope with respect to time for all seven cases are plotted in Fig. 9. The
217 peak magnitude within each period of oscillation is used as H_{amp} in the figures. Furthermore,
218 the scaled pressure envelopes predicted by the Vardy and Brown (1995, 1996 and 2003) for
219 smooth pipe turbulent flow and Vardy and Brown (2004) for rough pipe turbulent flows for
220 each test are also shown on the graphs. It is clear from the figure that in the early stages of the
221 transient: (i) the scaled peak pressure envelope from the experiments varies linearly with time
222 and (ii) the seven scenarios neatly collapse into a single line. This result indicates that the
223 damping model is valid within the early stages of the transient. This conclusion is consistent
224 with the previous results in Table 1 where the comparative plots of numerical and
225 experimental data showed the prediction of the damping envelope decreases in accuracy with
226 simulation time for current Re_0 based unsteady friction models—which encompasses the IAB
227 model by Brunone *et al.* (1991, 1995) and the WFB models by Vardy and Brown (1996, 2003)
228 and Zarzyki (2000). In other words, the frozen turbulence assumption based on the Re_0
229 condition adopted in these unsteady friction models is most valid in the early stage of the
230 transient and becomes progressively poor as time advances.

231

232 [add **Figure 9** at this place]

233

234 The result in Fig. 9 shows that while the scaled pressure envelopes converge into a
235 single line in the early stages of the transient, they diverge and become non-linear as the
236 transient proceeds. Such a departure from linearity and the loss of self similarity for large
237 time indicates that the predicted damping from the WFB unsteady friction model, which is
238 based on the assumption of frozen initial turbulence, begins to lose its accuracy at the later
239 stages of the transient. For a valve closure event, the mean flow velocity and turbulent
240 structure are expected to decay with time as the system oscillates towards a new mean state
241 (He and Jackson 2000, Ghidaoui *et al.* 2002). During the transient event, the turbulent
242 viscosity distribution and the thickness of the shear layer will change and the flow will
243 progressively lose dependence on Re_0 . While the frozen turbulent flow hypothesis is valid for
244 the early stages of the transient event (Ghidaoui *et al.* 2002), this assumption becomes
245 progressively violated at later stages.

246 Experimental investigation of turbulence behavior in transient flows in pipes (e.g., He
247 and Jackson 2000, He *et al.* 2011, and Vardy and Brown 2010) reported that the
248 instantaneous and not the pre-transient Reynolds number is the appropriate parameter that

249 collapses turbulent fluctuations and wall shear stress from different experiments into single
 250 curves. Using the instantaneous velocity amplitude instead of V_0 to define the local Reynolds
 251 number, \mathbf{Re}_t , as follows:

$$252 \quad \mathbf{Re}_t = \frac{V_{amp}(t)D}{\nu} = \frac{\left(V_0 e^{-K_r t / T_w}\right)D}{\nu} = \mathbf{Re}_0 e^{-K_r t / T_w} \quad (8)$$

253 and re-defining the total damping rate in terms of the local Reynolds number by inserting \mathbf{Re}_t
 254 in place of \mathbf{Re}_0 in Eqs. (A23) and (A22) respectively, gives:

255 (i) for smooth pipe flow case:

$$256 \quad K_r(t) \approx \begin{cases} \frac{f\mathbf{Re}_t}{2} \frac{T_w}{T_{dv}} + \sqrt{2 \frac{T_w}{T_{dv}}} & \text{if } \mathbf{Re}_0 \frac{T_w}{T_{dv}} \ll 1 \\ \frac{f\mathbf{Re}_t}{2} \frac{T_w}{T_{dv}} + \frac{1}{30.33(\mathbf{Re}_t)^{0.94}} \frac{T_{dv}}{T_w} & \text{otherwise} \end{cases} ; \quad (9)$$

$$= \begin{cases} \frac{f\mathbf{Re}_0 e^{-K_r t / T_w}}{2} \frac{T_w}{T_{dv}} + \sqrt{2 \frac{T_w}{T_{dv}}} & \text{if } \mathbf{Re}_0 \frac{T_w}{T_{dv}} \ll 1 \\ \frac{f\mathbf{Re}_0 e^{-K_r t / T_w}}{2} \frac{T_w}{T_{dv}} + \frac{1}{30.33\left(\mathbf{Re}_0 e^{-K_r t / T_w}\right)^{0.94}} \frac{T_{dv}}{T_w} & \text{otherwise} \end{cases}$$

257 (ii) for rough pipe flow case:

$$258 \quad K_r(t) \approx \frac{f\mathbf{Re}_t}{2} \frac{T_w}{T_{dv}} + 0.024 \left(\frac{\varepsilon}{D}\right)^{0.016} \left(\mathbf{Re}_t \frac{T_w}{T_{dv}}\right)^{-0.414}$$

$$= \frac{f\mathbf{Re}_0 e^{-K_r t / T_w}}{2} \frac{T_w}{T_{dv}} + 0.024 \left(\frac{\varepsilon}{D}\right)^{0.016} \left(\mathbf{Re}_0 e^{-K_r t / T_w} \frac{T_w}{T_{dv}}\right)^{-0.414} \quad (10)$$

259 To judge the appropriateness of the proposed re-scaling, the re-scaled amplitude
 260 $\frac{1}{-K_r(t)} \ln \frac{gH_{amp}(t)}{aV_0}$ versus time and with $K_r(t)$ given by Eq. (9) or (10) is plotted in Fig. 10.

261 The data from all seven cases now neatly collapses into a single linear curve. This collapse
 262 provides strong support for the fact that turbulent conditions within real transient flows are
 263 not frozen but change with the transient duration and that a relaxation of this assumption
 264 allows better match with the model at all times. As a consequence, it is proposed that the
 265 instantaneous, rather than the initial, Reynolds number is used in convolution integrals
 266 unsteady friction formulas for turbulent flows. The Vardy and Brown convolution unsteady
 267 friction model is modified accordingly and then implemented into a 1-D waterhammer model.
 268 The modified and original model are then applied and compared to the laboratory (case no. 3

269 in Table 1) and field data (case no. 6 in Table 1) and the results are shown in Figs. 11 and 12,
270 respectively. These cases are chosen because they are the ones for which the frozen
271 turbulence hypothesis is the least valid.

272

273 [add **Figures 10~12** at this place]

274

275 Figures 11 and 12 clearly show the gradual departure of the pressure head envelope (peaks)
276 by the original model from the experimental data. On the other hand, the results of modified
277 model are in better agreement with the experimental data throughout the entire simulation
278 time. Moreover, greater improvement resulted for the larger Re_0 case which represents a
279 practical field system application.

280

281 **Conclusions**

282 Many papers in recent years have focused on methods for estimating the unsteady shear stress
283 in transient flows and a popular type of physically-based unsteady friction model uses the
284 WFB relations derived in Vardy and Brown (1995, 1996, 2003) for smooth-pipe flows and in
285 Vardy and Brown (2004) for rough pipe flows. Despite the number of studies in this area, no
286 rigorous similitude analysis has been conducted on the model to (i) allow meaningful
287 comparisons of unsteady friction damping on transient responses of different pipeline
288 systems (ii) provide insight into the key parameters driving the damping of the head envelope
289 and (iii) identify limitations in the current model.

290 This paper theoretically derives an expression for the head envelope damping for
291 turbulent flow in smooth and rough pipes and provides general, encompassing and
292 theoretically-based dimensionless parameters, instead of the heuristically-based parameters in
293 Ghidaoui et al (2002) and Duan et al. (2012), that can be used to assess the importance of
294 unsteady friction in comparison to the quasi-steady component. The dimensionless
295 parameters allow the damping behavior from existing laboratory tests, the field tests
296 conducted as part of this research and the WFB models to be investigated and compared in a
297 coherent manner in a single graph. The key findings are as follows:

298 (1) The general trend that the importance of unsteady friction in rapidly decelerating
299 flows diminishes with Re_0 has been extended and validated for a larger number of initial
300 conditions.

301 (2) The accuracy of existing convolutional unsteady friction model, which are based
302 on the frozen eddy viscosity hypothesis such that the resulting convolution integrals are a

303 function of the pre-transient and not a time dependent Reynolds number, decreases with
304 simulation time of wave propagation.

305 (3) An improvement for the shortcoming in (2) is proposed and verified. It involves
306 the use of the instantaneous Reynolds number (Re_t) in lieu of the pre-transient Reynolds
307 number (Re_0) in the evaluation of the convolution integral models. The result indicates that
308 the modified unsteady friction model agrees better with data than the original model. The use
309 of Re_t is inspired by previous experimental investigation of turbulence behavior in transient
310 flows in pipes which show that the instantaneous and not the pre-transient Reynolds number
311 is the appropriate parameter for scaling turbulent fluctuations and wall shear stress.

312

313 **Acknowledgements:**

314 This research has been supported by: (i) Italian Ministry of Education, University and
315 Research under the Projects of Relevant National Interest "Advanced analysis tools for the
316 management of water losses in urban aqueducts", and "Tools and procedures for an advanced
317 and sustainable management of water distribution systems"; (ii) the Hong Kong Research
318 Grant Council under the projects nos. 612511 and 612910; and (iii) the Royal Society of
319 New Zealand with Marsden Grant UOC1153.

320

321 **References**

- 322 Adamkowski, A., and Lewandowski, M. (2006). Experimental examination of unsteady
323 friction models for transient pipe flow simulation. *Journal of Fluids Engineering*, ASME,
324 128(6), pp. 1351-1363.
- 325 Axworthy, DH, Ghidaoui, MS, and McInnis, DA. (2000). Extended thermodynamics
326 derivation of energy dissipation in unsteady pipe flow. *Journal of Hydraulic*
327 *Engineering*, ASCE, 126(4), pp. 276-287.
- 328 Bergant, A, Simpson, AR, and Vitkovsky, J. (2001). Developments in unsteady pipe flow
329 friction modelling. *Journal of Hydraulic Research*, IAHR, 39(3), pp. 249-257.
- 330 Brunone, B., Golia, U. M., and Greco, M. (1991). Some remarks on the momentum equations
331 for fast transients. In Cabrera, E. and Fanelli, M., editors, *Proc. "International Meeting*
332 *on Hydraulic Transients with Column Separation"*, 9th Round Table, IAHR, Valencia
333 (E), pp. 140-148.
- 334 Brunone, B., Golia, U.M., and Greco, M. (1995). Effects of two-dimensionality on pipe
335 transients modelling. *Journal of Hydraulic Engineering*, ASCE, 121(12), pp. 906-912.
- 336 Brunone, B., Ferrante, M., and Calabresi, F. (2001). High Reynolds number transients in a

337 pump rising main. Field tests and numerical modeling. In Lowdon, A., editor, *Proc., 4th*
338 *Int. Conference "Water Pipeline Systems"*, York (UK), BHR Group, pp. 339-348.

339 Brunone, B., Ferrante, M., and Calabresi, F. (2002). Discussion of "Evaluation of unsteady
340 flow resistances by quasi-2D or 1D models", by G. Pezzinga. *Journal of Hydraulic*
341 *Engineering*, ASCE, 128(6), pp. 646-647.

342 Brunone, B., Ferrante, M., and Cacciamani, M. (2004). Decay of pressure and energy
343 dissipation in laminar transient flow. *J. of Fluids Engineering*, ASME, 126(6), pp. 928-
344 934.

345 Brunone, B., and Golia, U.M. (2008). Discussion of "Systematic evaluation of one-
346 dimensional unsteady friction models in simple pipelines" by J.P. Vitkovsky, A. Bergant,
347 A.R. Simpson, and M. F. Lambert. *J. of Hydraulic Engineering*, ASCE, 134(2), pp. 282-
348 284.

349 Duan, H.F., Ghidaoui, M.S., Lee, P.J. and Tung, Y.K. (2010). Unsteady friction and visco-
350 elasticity in pipe fluid transients. *Journal of Hydraulic Research*, IAHR, 48(3), pp. 354-
351 362.

352 Duan, H.F., Ghidaoui, M.S. Lee, P J and Tung, Y K. (2012). Relevance of unsteady friction
353 to pipe size and length in pipe fluid transients. *Journal of Hydraulic Engineering*, ASCE,
354 138(2), pp. 154-166.

355 Ghidaoui, MS, Mansour, SGS, and Zhao, M. (2002). Applicability of quasisteady and
356 axisymmetric turbulence models in water hammer. *Journal of Hydraulic Engineering*,
357 ASCE, 128(10), pp. 917-924.

358 Ghidaoui, M.S. and Mansour, S. (2002). Efficient Treatment of the Vardy-Brown Unsteady
359 Shear in Pipe Transients. *Journal of Hydraulic Engineering*, ASCE, 128(1), pp. 102-112.

360 Ghidaoui, MS, Zhao, M., McInnis, DA, and Axworthy, DH. (2005). A review of water
361 hammer theory and practice. *Applied Mechanics Reviews*, 58(1), pp. 49-76.

362 He, S., and Jackson, J. D. (2000). A study of turbulence under conditions of transient flow in
363 a pipe. *Journal of Fluid Mechanics*, 408, pp. 1-38.

364 He, S., Ariyaratne, C. and Vardy, A.E. (2011). Wall shear stress in accelerating turbulent
365 pipe flow. *Journal of Fluid Mechanics*, 685, pp. 440-460.

366 Holmboe, EL, and Rouleau, WT. (1967). The effect of viscous shear on transients in liquid
367 lines. *Journal of Basic Engineering*, ASME, 89(1), pp. 174-180.

368 Mitosek, M., and Szymkiewicz, R. (2012). Wave damping and smoothing in the unsteady
369 pipe flow. *Journal of Hydraulic Engineering*, ASCE, 138(7), pp. 619-628.

370 Pezzinga, G. (2009). Local balance unsteady friction model. *Journal of Hydraulic*

371 *Engineering*, ASCE, 135(1), pp. 45-56.

372 Silva-Araya, WF, and Chaudhry, MH. (2001). Unsteady friction in rough pipes. *Journal of*
373 *Hydraulic Engineering*, ASCE, 127(7), pp. 607-618.

374 Silva-Araya, WF, and Chaudhry, MH. (1997). Computation of energy dissipation in transient
375 flow. *Journal of Hydraulic Engineering*, ASCE, 123(2), pp. 108-115.

376 Stephens M., Simpson A. R., Lambert M. F., and Vlkovsky J. P. (2005). Field measurement
377 of unsteady friction effects in a trunk transmission pipeline. *Proc. Int. Conf. of 7th*
378 *Annual Symposium on Water Distribution Systems Analysis*, Anchorage, Alaska, USA,
379 15-19 May, 2005.

380 Storli, P-T, and Nielsen, TK. (2011a). Transient friction in pressurized pipes. ii: two-
381 coefficient instantaneous acceleration-based model. *Journal of Hydraulic Engineering*,
382 ASCE, 137(6), pp. 679-695.

383 Storli, P-T, and Nielsen, TK. (2011b). Transient friction in pressurized pipes III: investigation
384 of the EIT model based on position-dependent coefficient approach in MIAB model.
385 *Journal of Hydraulic Engineering*, ASCE, 137(9), pp. 1047-1053.

386 Trikha, AK. (1975). An efficient method for simulating frequency-dependent friction in
387 transient liquid flow. *Journal of Fluids Engineering*, ASME, 97(1), pp. 97-105.

388 Vardy, AE and Brown, JMB. (1995). Transient, turbulent, smooth pipe friction. *Journal of*
389 *Hydraulic Research*, IAHR, 33(4), pp. 435-456.

390 Vardy, AE and Brown, JMB. (1996). On turbulent, unsteady, smooth-pipe friction. *Proc.,*
391 *7th Int. Conf. on "Pressure Surges and Fluid Transients in Pipelines and Open*
392 *Channels"*, Harrogate (UK), BHR Group, pp. 289-311.

393 Vardy, AE and Brown, JMB. (2003). Transient turbulent friction in smooth pipe flows.
394 *Journal of Sound and Vibration*, 259(5), pp. 1011-1036.

395 Vardy, AE and Brown, JMB. (2004). Transient turbulent friction in fully rough pipe flows.
396 *Journal of Sound and Vibration*, 270(2), pp. 233-257.

397 Vardy, AE, and Brown, JMB. (2010). Influence of time-dependent viscosity on wall shear
398 stresses in unsteady pipe flows. *Journal of Hydraulic Research*, IAHR, 48(2), pp. 225-
399 237.

400 Vitkovský, J., Stephens, M., Bergant, A., Simpson, A., and Lambert, M. (2006). Numerical
401 error in weighting function-based unsteady friction models for pipe transients. *Journal of*
402 *Hydraulic Engineering*, ASCE, 132(7), pp. 709-721.

403 Zarzycki, Z. (2000). On weighting function for wall shear stress during unsteady turbulent
404 pipe flow. *Proc., 8th Int. Conf. on Pressure Surges*, The Hague (NL), BHR Group, pp.

405 529-543.

406 Zhao, M., Ghidaoui, M.S., and Kolyshkin, A. A. (2007). Perturbation dynamics in unsteady
407 pipe flows. *Journal of Fluid Mechanics*, 570, pp. 129-154.

408 Zielke, W. (1968). Frequency-dependent friction in transient pipe flow. *Journal of Basic*
409 *Engineering*, ASME, 90(1), pp. 109-115.

410

411 **Appendix I: Analytical Solution of Transient Oscillating Envelope**

412 The 1-D waterhammer equations in the dimensionless form used for this study are (Ghidaoui
413 *et al.* 2005, Duan *et al.* 2012):

$$414 \quad \frac{\partial H^*}{\partial t^*} + \frac{aQ_0}{gAH_0} \frac{\partial Q^*}{\partial x^*} = 0, \quad (A1)$$

$$415 \quad \frac{\partial Q^*}{\partial t^*} + \frac{gAH_0}{aQ_0} \frac{\partial H^*}{\partial x^*} + \frac{fLQ_0}{aDA} Q^* + \frac{4\pi\nu L}{aA} \int_0^{t^*} W(t^{**}) \frac{\partial Q^*}{\partial t^{**}} dt^{**} = 0. \quad (A2)$$

416 where Q = flow discharge; x = the distance along pipeline; and t' is a dummy time variable;
417 other symbols have been defined in the previous text; superscript “*” is representing
418 dimensionless form, and the following dimensionless quantities are considered:

$$419 \quad H^* = \frac{H}{H_0}; \quad Q^* = \frac{Q}{Q_0}; \quad t^* = \frac{t}{T_w}; \quad \text{and} \quad x^* = \frac{x}{L}. \quad (A3)$$

420 As indicated in Eq. (1) in the text, the total shear stress (τ_w) in transients has been
421 separated into two parts to isolate the impacts of quasi-steady and unsteady friction
422 components in Eq. (A2) above: a quasi-steady part (τ_{ws}) and an unsteady part (τ_{wu}). Moreover,
423 the quasi-steady part relating to the average velocity is represented by the classic Darcy-
424 Weisbach equation (Ghidaoui *et al.* 2005), and for the possibility of analytical derivation, it
425 has been linearized for relatively small transient flow as (Duan *et al.* 2012):

$$426 \quad \tau_{ws} = \frac{\rho f Q^2}{4A^2} \approx \frac{\rho f Q_0}{4A^2} (Q_0 + q) = \frac{\rho f Q_0}{4A^2} Q, \quad (A4)$$

427 where q is the oscillation of unsteady flow in pipeline relative to steady-state (pre-transient
428 state), and $q = Q - Q_0$. Theoretically Eq. (A4) is derived for $q \ll Q_0$, however it has also been
429 validated in Duan *et al.* (2012) by using 2-D numerical simulations that Eq. (A4) is also valid
430 for the transients caused by the full closure of end valve.

431 On the other hand, the unsteady part is related to the fluid acceleration by the
432 convolution integral relations (i.e., WFB models) such as the one in Zielke (1968) for laminar
433 flows and Vardy and Brown (1995, 1996, 2003, and 2004) for turbulent flows. The general
434 form of this WFB model is:

435
$$\tau_{wu} = \frac{4\rho\nu}{DA} \int_0^t W(t-t') \frac{\partial Q(t')}{\partial t'} dt', \quad (\text{A5})$$

436 For laminar flow regime, the weighting function can be expressed by exponential relations
 437 and details refer to Zielke (1968) or Ghidaoui *et al.* (2005). While for the turbulent case, an
 438 approximated expression of the weighting function in a dimensionless form has been derived
 439 by Vardy and Brown (1995, 1996, 2003, and 2004):

440
$$W(t^*) = \alpha' \frac{e^{-\beta' t^*}}{\sqrt{\pi t^*}}, \quad (\text{A6})$$

441 where α' , β' are coefficients relating to transient events and the pipeline system under
 442 investigation. Specifically, for smooth pipe flows (Vardy and Brown 1995, 1996),

443
$$\alpha' = \frac{1}{4} \sqrt{\frac{T_{dv}}{T_w}}, \text{ and } \beta' = 0.54 k_{Re_0} \frac{T_w}{T_{dv}}, \quad (\text{A7})$$

444 where $T_w = L/a$ is longitudinal wave timescale, $T_{dv} = D^2/\nu$ is radial viscous diffusion timescale,
 445 and $k_{Re_0} = (\mathbf{Re}_0)^{1.0543/(Re_0^{0.05})}$ is initial Reynolds number based coefficient.

446 For fully rough pipe flows (Vardy and Brown 2003, 2004), the coefficients are,

447
$$\alpha' = 0.0091 \left(3 \frac{\varepsilon}{D}\right)^{0.39} \sqrt{\mathbf{Re}_0 \frac{T_{dv}}{T_w}}, \text{ and } \beta' = 1.408 \left(\frac{\varepsilon}{D}\right)^{0.41} \mathbf{Re}_0 \frac{T_w}{T_{dv}}, \quad (\text{A8})$$

448 To investigate the effect of different parameters of pipeline system and transient
 449 events on the friction (steady and unsteady) induced damping of the transient envelope,
 450 similar analytical analysis process can be conducted with the aid of applying Fourier
 451 transform to system Eqs. (A1) and (A2). The obtained results are,

452
$$i\omega^* \hat{H}^* + \frac{aQ_0}{gAH_0} \frac{\partial \hat{Q}^*}{\partial x^*} = 0, \quad (\text{A9})$$

453
$$i\omega^* \hat{Q}^* + \frac{gAH_0}{aQ_0} \frac{\partial \hat{H}^*}{\partial x^*} + \frac{fLQ_0}{aDA} \hat{Q}^* + \frac{4\pi\nu L}{aA} \frac{i\alpha'\omega^*}{\sqrt{\beta'+i\omega^*}} \hat{Q}^* = 0, \quad (\text{A10})$$

454 where $\hat{H}^*(x^*, \omega^*)$, $\hat{Q}^*(x^*, \omega^*)$ are the amplitudes of head and discharge in the frequency
 455 domain, ω^* is angular frequency of transient signals.

456 By combining Eqs. (A9) and (A10), the resultant equations for pressure head and
 457 discharge are,

458
$$\frac{\partial^2 \hat{H}^*}{\partial (x^*)^2} + C^* \hat{H}^* = 0, \text{ and } \frac{\partial^2 \hat{Q}^*}{\partial (x^*)^2} + C^* \hat{Q}^* = 0, \quad (\text{A11})$$

459 where C^* is a lumped parameter for wave propagation, and,

460
$$C^* = (\omega^*)^2 \left(1 - i \frac{fLQ_0}{aDA\omega^*} + \frac{4\pi\nu L}{aA} \frac{\alpha'}{\sqrt{\beta' + i\omega^*}} \right). \quad (\text{A12})$$

461 It is easy to obtain the form of the solution to Eq. (A11) given by (Duan *et al.* 2012),

462
$$\hat{H}^*(x^*, \omega^*) = \hat{H}_0^* e^{-K_0 x^*}, \quad \text{and} \quad \hat{Q}^*(x^*, \omega^*) = \hat{Q}_0^* e^{-K_0 x^*}, \quad (\text{A13})$$

463 where \hat{H}_0^* , \hat{Q}_0^* relate to the initial values (head and discharge); and $K_0 = K_{r0} + iK_{i0}$ with K_{r0}
464 and K_{i0} the parameters of the wave envelope decay and phase shift, respectively, and,

465
$$K_{r0} = \sqrt{\frac{\sqrt{(\Omega_1)^2 + (\Omega_2)^2} - \Omega_1}{2}}; \quad K_{i0} = \sqrt{\frac{\sqrt{(\Omega_1)^2 + (\Omega_2)^2} + \Omega_1}{2}}, \quad (\text{A14})$$

466 where,

467
$$\Omega_1 = 1 + \frac{4\pi\nu L\alpha'}{aA} \sqrt{\frac{\sqrt{(\beta')^2 + (\omega^*)^2} + \beta'}{2((\beta')^2 + (\omega^*)^2)}}; \quad \Omega_2 = \frac{fLQ_0}{aDA\omega^*} + \frac{4\pi\nu L\alpha'}{aA} \sqrt{\frac{\sqrt{(\beta')^2 + (\omega^*)^2} - \beta'}{2((\beta')^2 + (\omega^*)^2)}}. \quad (\text{A15})$$

468 Consequently, it is now clear from Eqs. (A13) through (A15) that the transient oscillation
469 responses for pressure head and discharge are damping exponentially in the frequency
470 domain. Meanwhile, in the single pipe the wave propagation period $T_w \sim L/a$ is corresponding
471 to the distance of wave propagating cycles along the pipeline, i.e., $x^* \sim 1$ in the dimensionless
472 form. Therefore the damping factor of the transient envelope for each wave period is
473 approximated by e^{-K_0} . As a result for the n^{th} period (or n^{th} envelope location), the damped
474 transient envelope becomes,
475

476
$$H_{amp}(n) = H_{amp0} e^{-nK_{r0}}, \quad \text{and} \quad Q_{amp}(n) = Q_{amp0} e^{-nK_{r0}}, \quad (\text{A16})$$

477 where subscript “amp” denotes amplitude, n is number of wave period, H_{amp0} , $Q_{amp0} =$
478 quantities relating to initial (pre-transient) state conditions, and $H_{amp0} = \frac{aV_0}{g}$, $Q_{amp0} = Q_0$ for
479 the transients caused by sudden valve closure and pump failure considered in this study. In
480 terms of wave time, the result becomes,

481
$$H_{amp}(t) = \frac{aV_0}{g} e^{-K_{r0} \frac{t}{T_w}}, \quad \text{and} \quad Q_{amp}(t) = Q_0 e^{-K_{r0} \frac{t}{T_w}}, \quad (\text{A17})$$

482 The validity of the approximate form of Eq. (A17) is validated in the paper through the field
483 tests of this study as well as other data from the literature.

484 As in Eq. (A2), the decay parameter K_{r0} is divided into two parts to describe the
485 individual contribution of steady and unsteady friction to the transient envelope damping, as,

486
$$K_{r,0} = K_{r,\delta} + K_{r,\theta}. \quad (\text{A18})$$

487 Meanwhile, to better understand the impacts of system parameters and flow conditions on the
 488 importance of friction damping, the decay parameter $K_{r,0}$ in Eq. (A14) can be further
 489 simplified as conducted in Duan *et al.* (2012),

490
$$K_{r,0} = K_{rs,0} + K_{ru,0} \approx \frac{fM}{2} \frac{L}{D} + 8C_{\alpha\beta} \frac{M}{Re_0} \frac{L}{D} = \frac{fRe_0}{2} \frac{T_w}{T_{dv}} + 8C_{\alpha\beta} \frac{T_w}{T_{dv}}, \quad (\text{A19})$$

491 where $C_{\alpha\beta}$ is coefficient relating to α' and β' in Eq. (A7) for smooth case and Eq. (A8) for
 492 rough case, and applying $\omega^* \sim 1$ for the case of fast valve closure or sudden pump stoppage,

493
$$C_{\alpha\beta} = \alpha' \sqrt{\frac{\sqrt{1+(\beta')^2} - \beta'}{2[1+(\beta')^2]}}. \quad (\text{A20})$$

494 Specifically, for the rough cases of the given single pipe in this study, it can be approximately
 495 obtained that,

496
$$C_{\alpha\beta} \approx 0.26 \ln(\beta)^{0.913}, \quad (\text{A21})$$

497 with a fitness of this approximation to original Eq. (A20), $R^2 = 0.95$. As a result, for fully
 498 rough pipe flow case (e.g., the field tests of this study):

499
$$K_{r,0} = K_{rs,0} + K_{ru,0} \approx \frac{fM}{2} \frac{L}{D} + 0.024 \left(\frac{\varepsilon}{D}\right)^{0.016} \left(\frac{M}{D}\right)^{-0.414} = \frac{fRe_0}{2} \frac{T_w}{T_{dv}} + 0.024 \left(\frac{\varepsilon}{D}\right)^{0.016} \left(Re_0 \frac{T_w}{T_{dv}}\right)^{-0.414}. \quad (\text{A22})$$

500 Furthermore for clarity and completeness, the results for smooth pipe flow case summarized
 501 from Duan *et al.* (2012) are also shown here as,

503
$$K_{r,0} = K_{rs,0} + K_{ru,0} \approx \begin{cases} \frac{fM}{2} \frac{L}{D} + \sqrt{2 \frac{L}{D} \frac{M}{Re_0}} & \text{if } \frac{M}{D} \ll 1 \\ \frac{fM}{2} \frac{L}{D} + \frac{(Re_0)^{0.063}}{30.33} \frac{D}{L} \frac{1}{M} & \text{otherwise} \end{cases}, \quad (\text{A23})$$

$$= \begin{cases} \frac{fRe_0}{2} \frac{T_w}{T_{dv}} + \sqrt{2 \frac{T_w}{T_{dv}}} & \text{if } Re_0 \frac{T_w}{T_{dv}} \ll 1 \\ \frac{fRe_0}{2} \frac{T_w}{T_{dv}} + \frac{1}{30.33 (Re_0)^{0.94}} \frac{T_{dv}}{T_w} & \text{otherwise} \end{cases}$$

504 It is necessary to note that Eqs. (A22) and (A23) are simplified for specific conditions
 505 such as the timescale ratio $\frac{T_w}{T_{dv}} \ll 1$ (Duan *et al.* 2012), and for obtaining general conclusions
 506 the original full version of Eqs. (A14) and (A15) should be used.

507

508

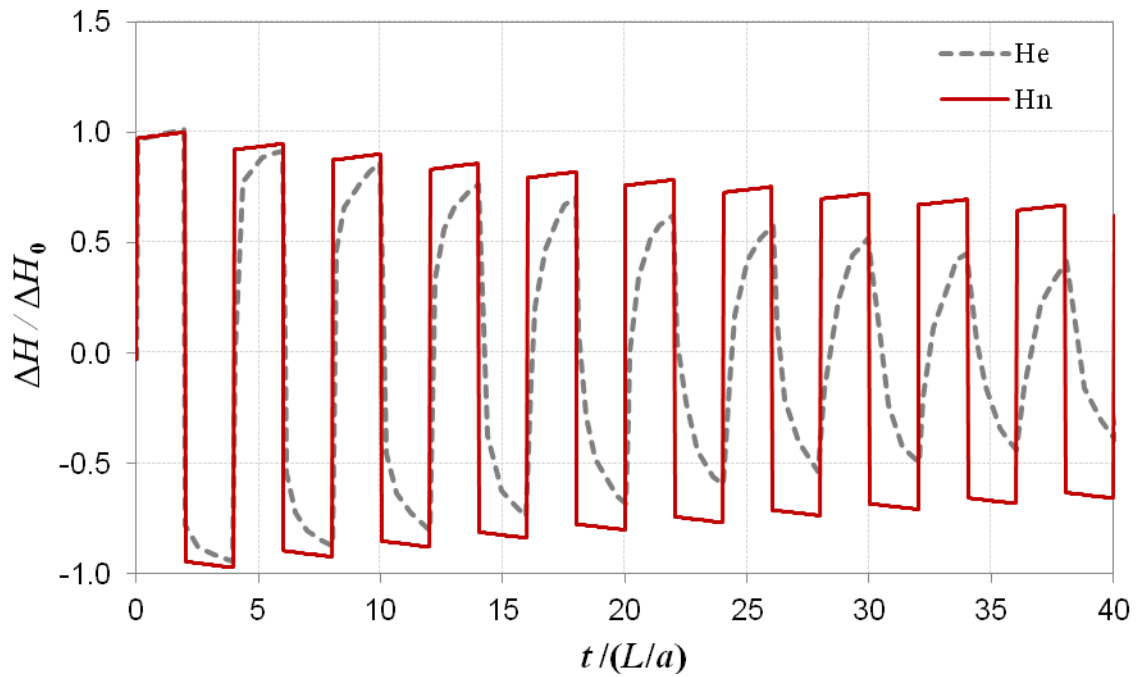
509
510
511
512
513
514
515
516
517

Table 1: Main characteristics of experimental tests

Test pipe system	Test no.	L/D	f	M	Re_0	Flow regime	I	K_{ru0}/K_{rs0}
Laboratory system (from Adamkowski and Lewandowski, 2006)	1	6132	0.036	0.00026	5731	<i>Smooth</i>	0.06	1.192
	2	6132	0.030	0.00049	10634	<i>Smooth</i>	0.09	0.431
	3	6132	0.027	0.00072	15843	<i>Smooth</i>	0.12	0.221
Field system tested by the authors of this study	4	16038	0.037	0.00031	97584	<i>Rough</i>	0.18	0.124
	5	16038	0.037	0.00043	136139	<i>Rough</i>	0.26	0.081
	6	16038	0.037	0.00076	239957	<i>Rough</i>	0.45	0.036
	7	16038	0.037	0.00124	386379	<i>Rough</i>	0.72	0.018

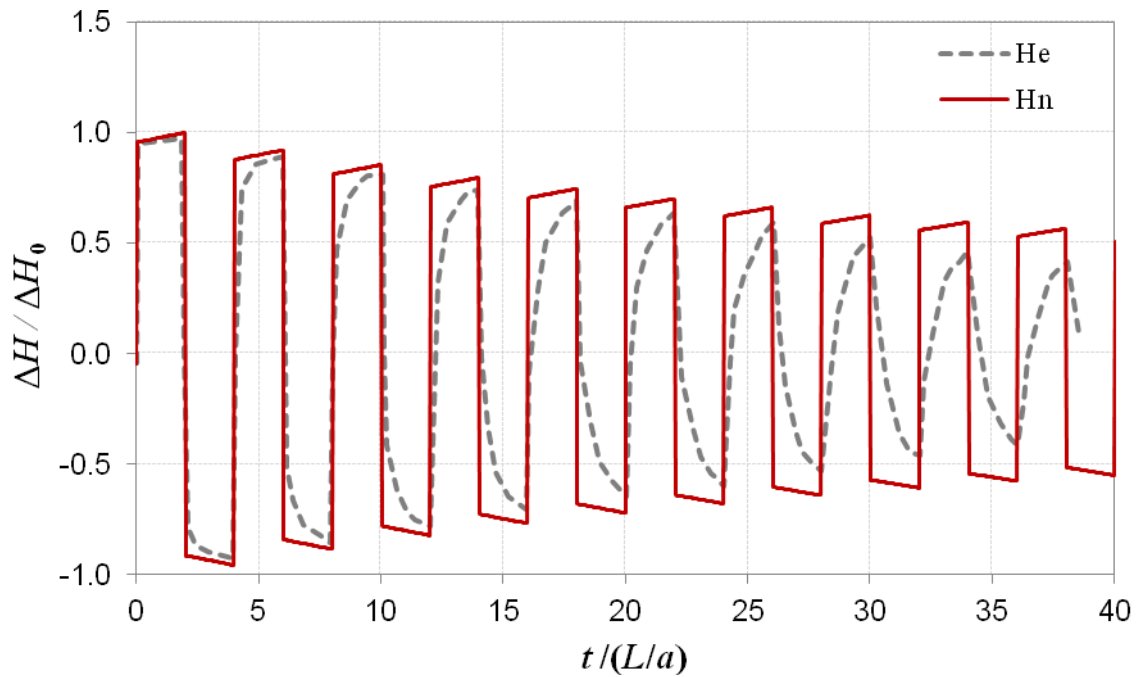
518
519
520
521
522
523
524
525
526
527
528
529
530
531
532
533
534
535
536
537
538

539
540



541
542
543
544
545

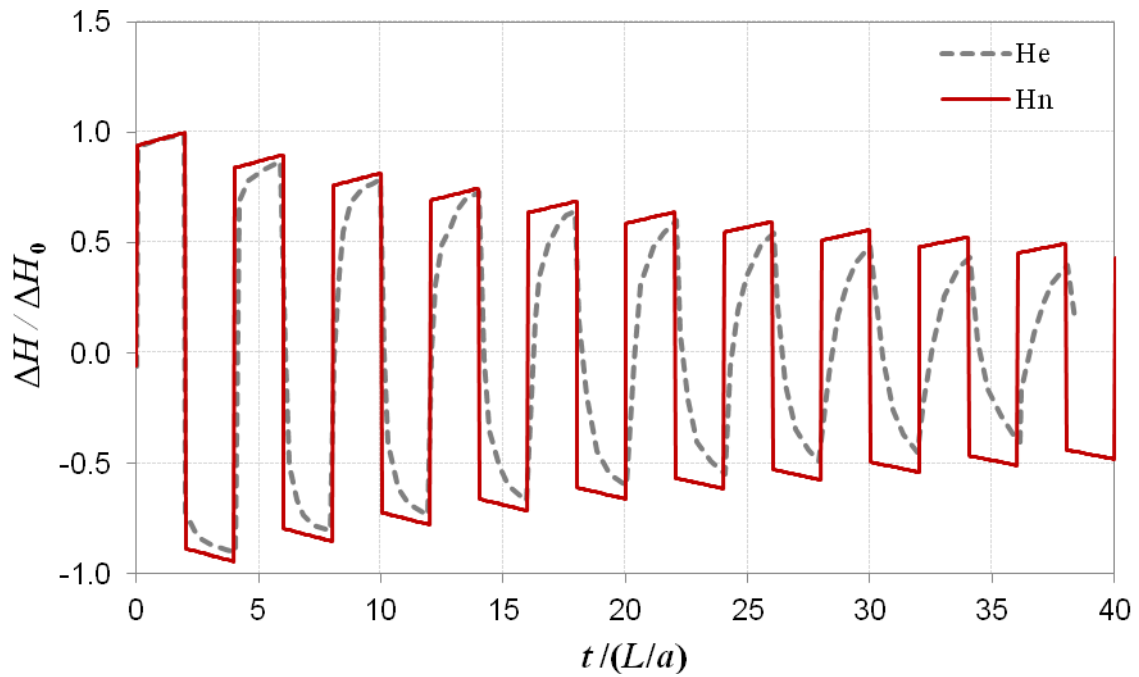
Figure 1: Experimental and numerical pressure signals for laboratory test with $Re_0 = 5731$ (test no. 1 in Table 1; H_n is numerical result based on 1-D model, and H_e is experimental data retrieved from Adamkowski and Lewandowski, 2006)



546
547
548
549
550
551
552

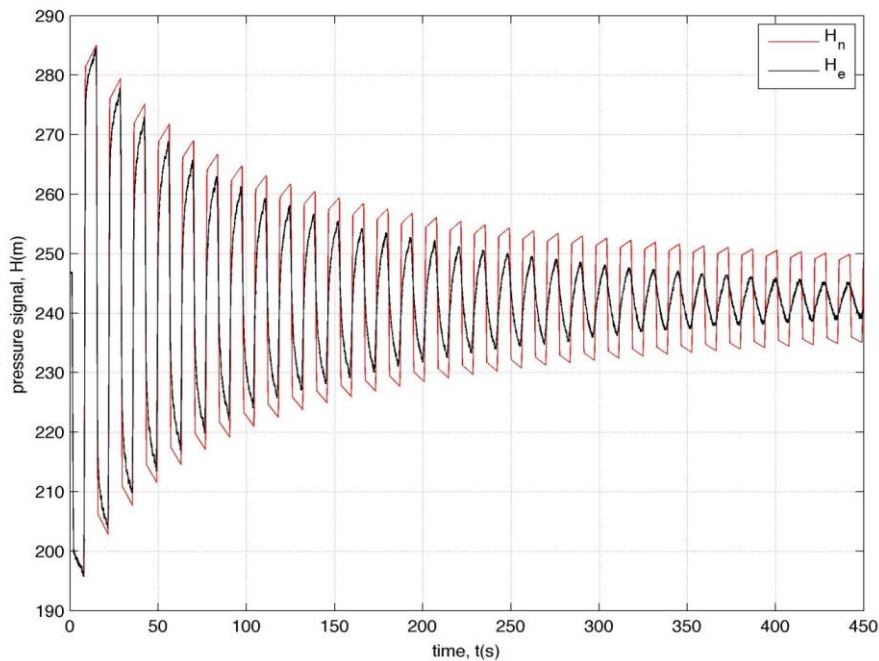
Figure 2: Experimental and numerical pressure signals for laboratory test with $Re_0 = 10634$ (test no. 2 in Table 1; H_n is numerical result based on 1-D model, and H_e is experimental data retrieved from Adamkowski and Lewandowski, 2006)

553
554



555
556
557
558
559

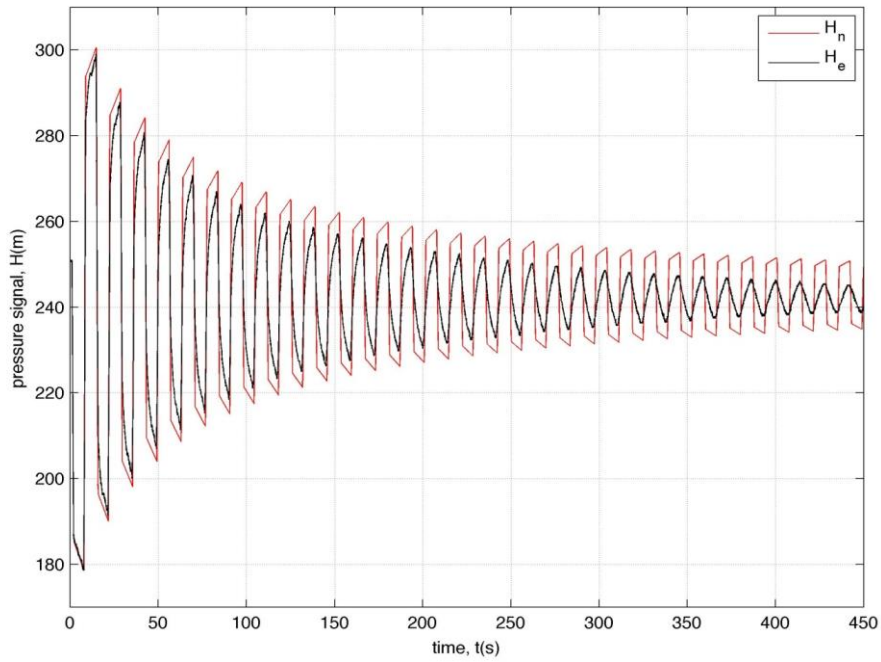
Figure 3: Experimental and numerical pressure signals for laboratory test with $Re_0 = 15843$ (test no. 3 in Table 1; H_n is numerical result based on 1-D model, and H_e is experimental data retrieved from Adamkowski and Lewandowski, 2006)



560
561
562
563
564
565

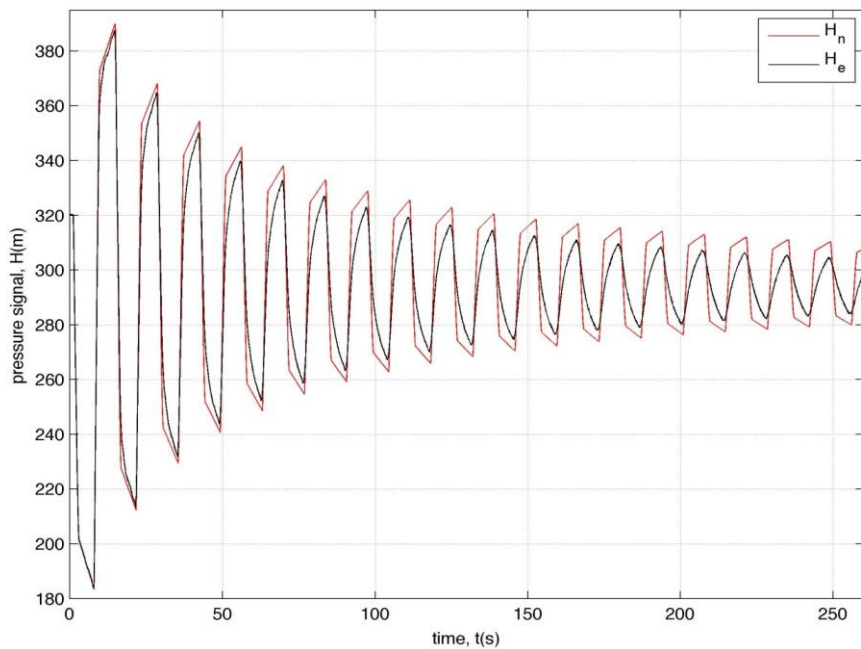
Figure 4: Experimental and numerical pressure signals for field test due to pump shutdown with $Re_0 = 97584$ (test no. 4 in Table 1; H_n is numerical result based on 1-D model, and H_e is experimental data)

566
567



568
569
570
571

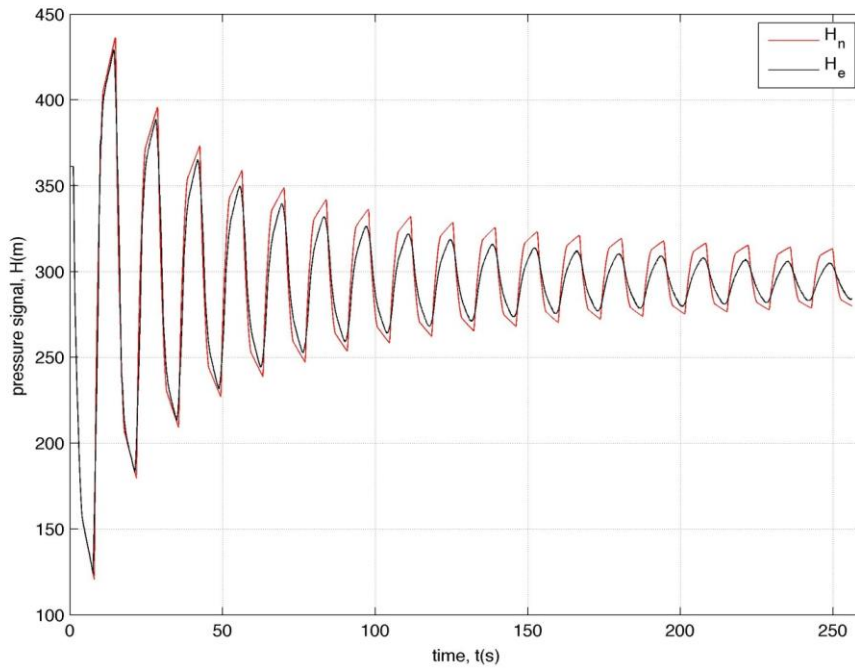
Figure 5: Experimental and numerical pressure signals for field test due to pump shutdown with $Re_0 = 136139$ (test no. 5 in Table 1; H_n is numerical result based on 1-D model, and H_e is experimental data)



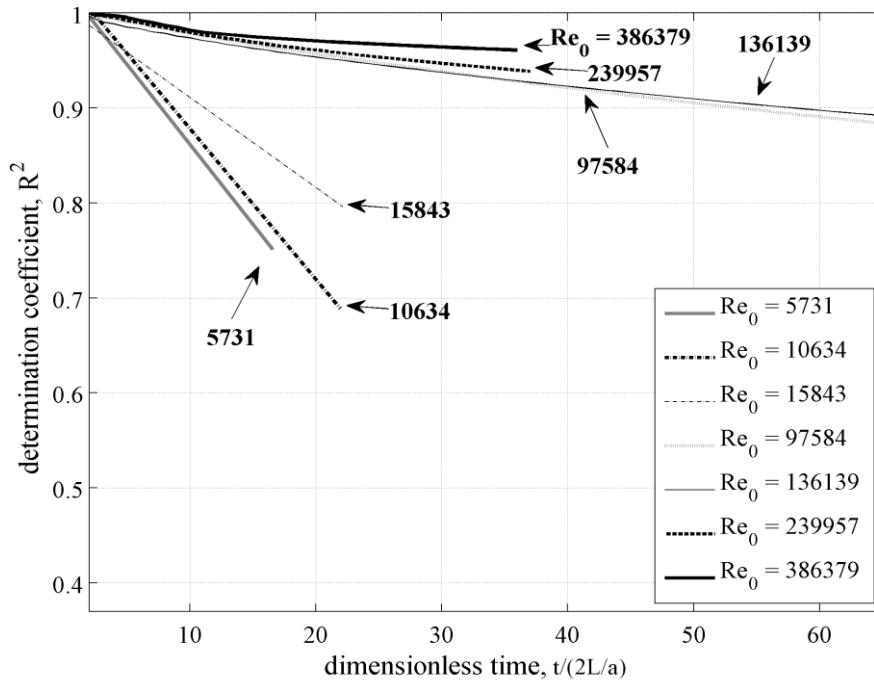
572
573
574
575
576
577
578

Figure 6: Experimental and numerical pressure signals for field test due to pump shutdown with $Re_0 = 239957$ (test no. 6 in Table 1; H_n is numerical result based on 1-D model, and H_e is experimental data)

579
580

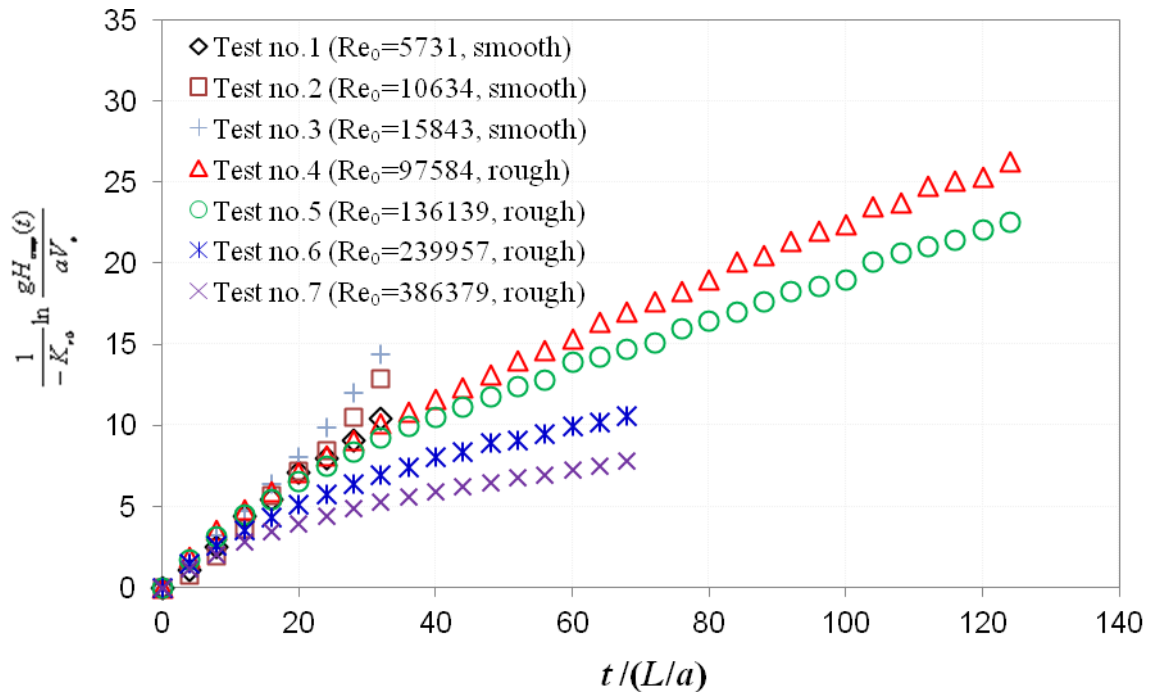


581
582 **Figure 7:** Experimental and numerical pressure signals for field test due to pump shutdown
583 with $Re_0 = 386379$ (test no. 7 in Table 1; H_n is numerical result based on 1-D model, and H_e
584 is experimental data)
585



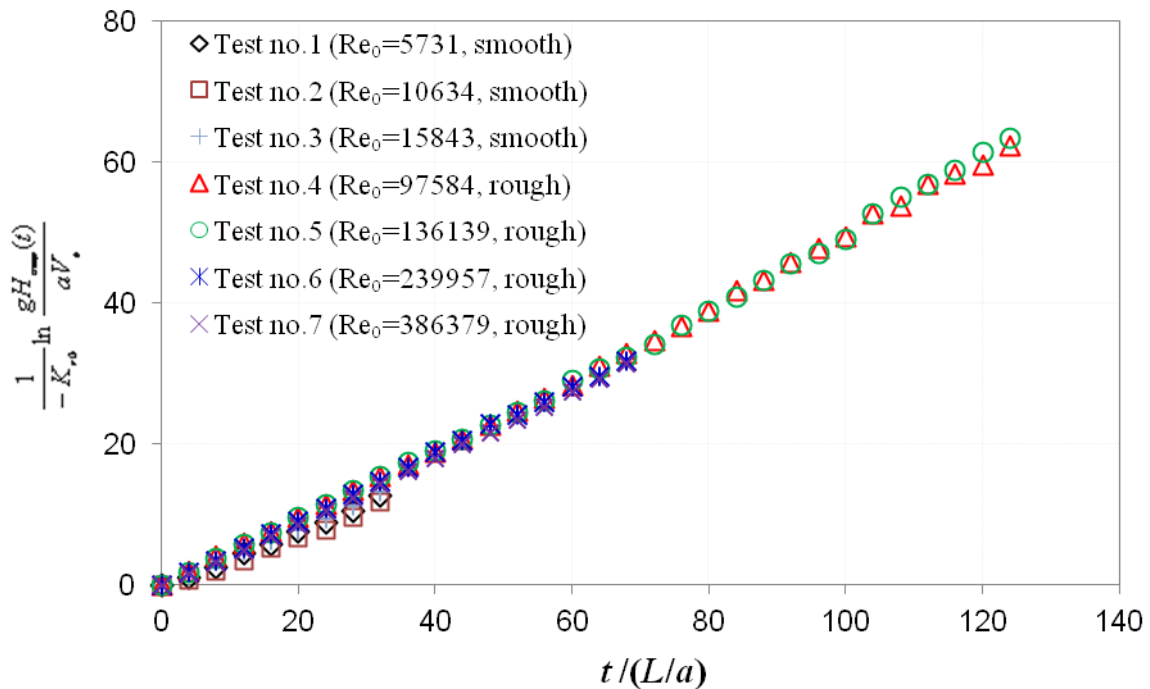
586
587 **Figure 8:** The determination coefficient, R^2 , vs. the dimensionless time
588
589
590

591
592



593
594
595
596
597

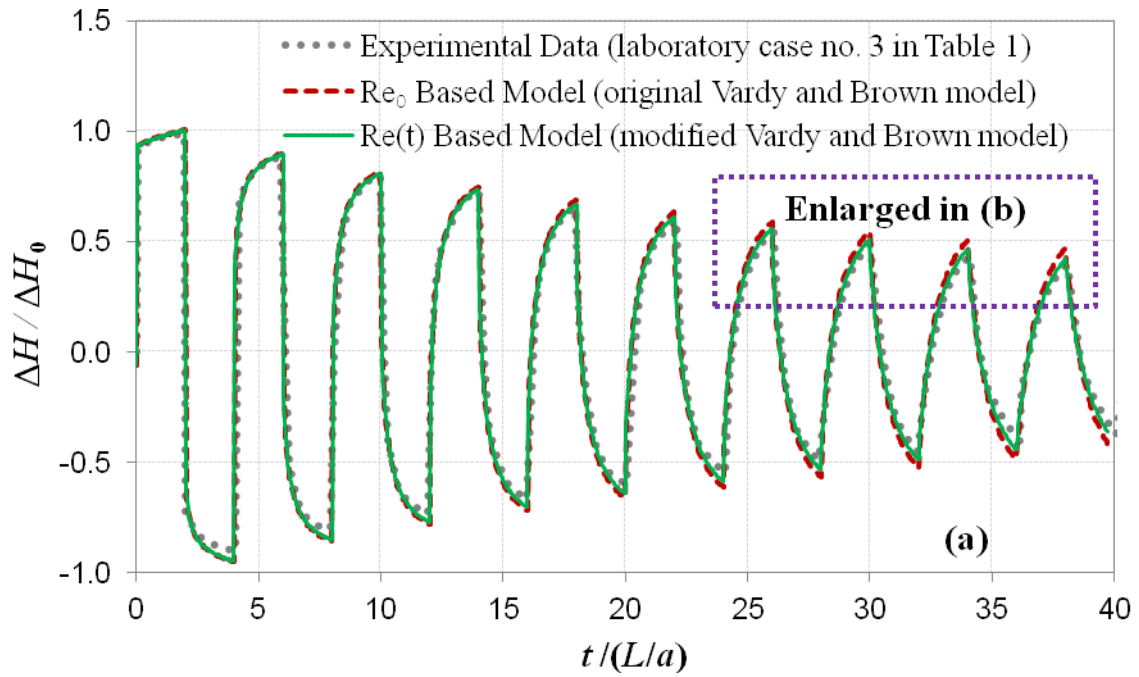
Figure 9: The variation of rescaled pressure amplitude with time using Re_0 for test cases in Table 1



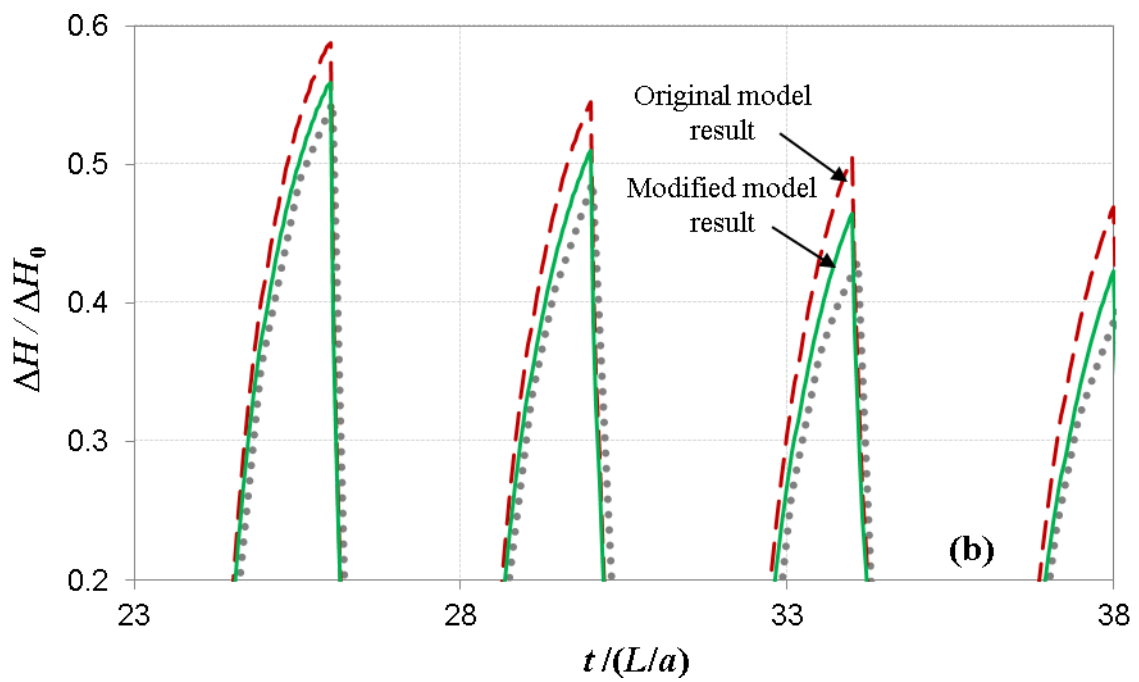
598
599
600
601
602
603

Figure 10: The variation of rescaled pressure amplitude with time using time dependent Re_t for test cases in Table 1

604
605



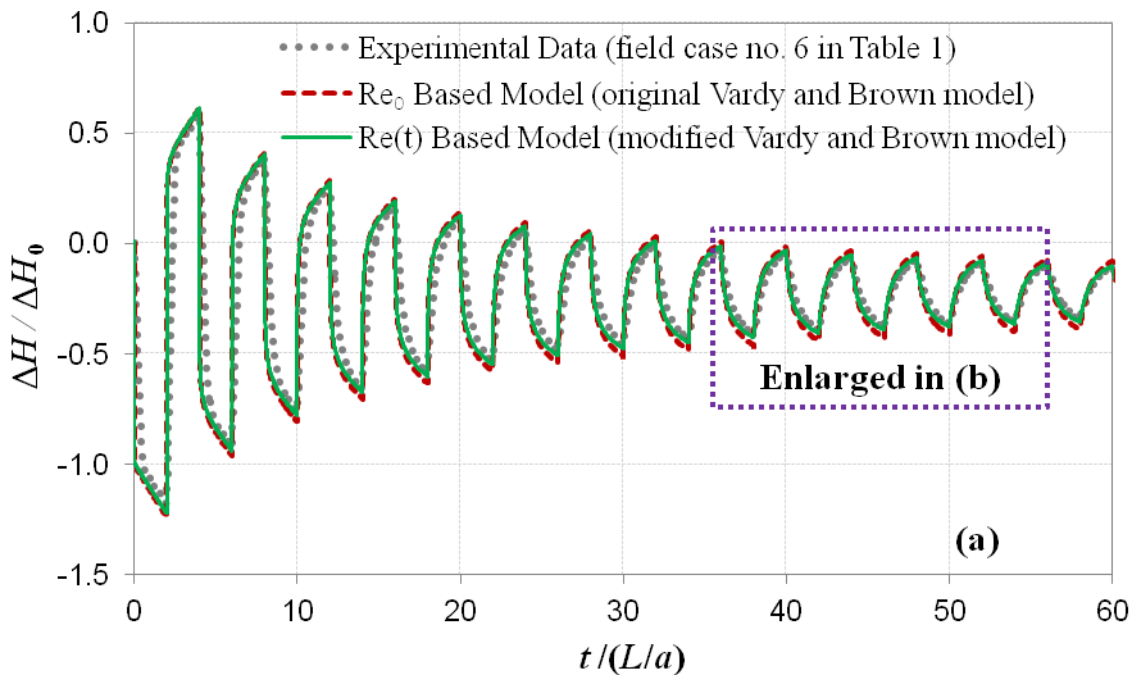
606



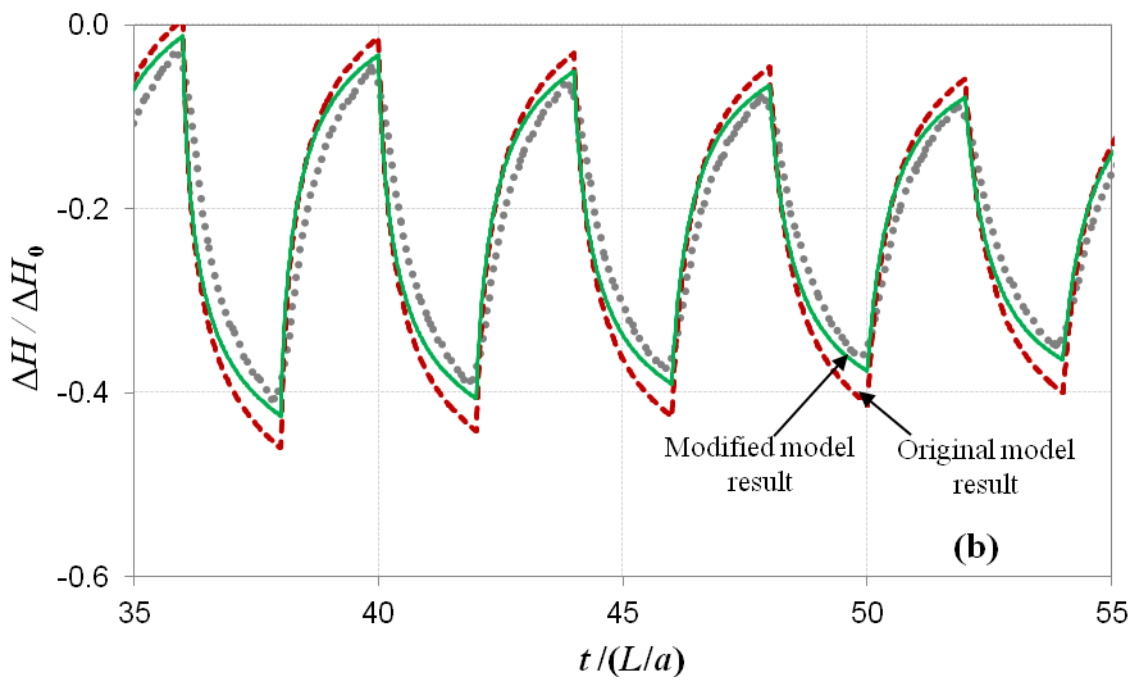
607
608
609
610
611
612
613
614
615
616
617

Figure 11: Experimental data and numerical results of pressure head traces based on different models for laboratory test case no. 3 in Table 1 ($Re_0=15843$)

618
619



620



621
622
623
624
625

Figure 12: Experimental data and numerical results of pressure head traces based on different models for field test case no. 6 in Table 1 ($Re_0=239957$)